



Published in final edited form as:

J Magn Reson Imaging. 2014 December ; 40(6): 1342–1346. doi:10.1002/jmri.24498.

From Unicuspid to Quadricuspid: Influence of Aortic Valve Morphology on Aortic 3D Hemodynamics

Pegah Entezari, M.D.¹, Susanne Schnell, Ph.D.¹, Riti Mahadevia, B.S.¹, Chris Malaisrie, M.D.², Patrick McCarthy, M.D.², Marla Mendelson, M.D.⁴, Jeremy Collins, M.D.¹, James C. Carr, M.D.¹, Michael Markl, Ph.D.^{1,3}, and Alex J. Barker, Ph.D.¹

¹ Departments of Radiology and Biomedical Engineering, Northwestern University, Chicago, IL, USA

² Departments of Radiology, Northwestern University, Chicago, IL, USA

³ Department of Neurological Surgery, Northwestern University, Chicago, IL, USA

⁴ Departments of Neurological Surgery and Radiology, Northwestern University, Chicago, IL, USA

Abstract

Purpose—To assess the impact of aortic valve morphology on aortic hemodynamics between normal tricuspid and congenitally anomalous aortic valves ranging from unicuspid to quadricuspid morphology.

Materials and Methods—Aortic 3D blood flow was evaluated by 4D flow MRI in 14 healthy volunteers with normal trileaflet valves and 14 patients with unicuspid (n=3), bicuspid (n=9, 3 ‘true’ bicuspid, 3 right-left (RL), 3 right-non (RN) coronary leaflet fusion, and quadricuspid aortic valves (n=2). Data analysis included the co-registered visualization of aortic valve morphology with systolic 3D blood flow. The influence of valve morphology on aortic hemodynamics was quantified by valve flow angle.

Results—All RL-BAV were associated with flow jets directed towards the right anterior aortic wall while RN-fusion and unicuspid valves resulted in flow jet patterns towards the right-posterior or posterior wall. Flow angles were clearly influenced by valve morphology ($47^{\circ} \pm 10$, $28^{\circ} \pm 2$, $29^{\circ} \pm 18$, $18^{\circ} \pm 12$, $15^{\circ} \pm 2$ for unicuspid, true BAV, RN-BAV, RL-BAV, quadricuspid valves) and increased compared to controls ($7.2^{\circ} \pm 1.1$, $p=0.001$).

Conclusions—Altered 3D aortic hemodynamics are impacted by the morphology of congenitally malformed aortic valves.

Keywords

4D flow MRI; aortic valve; unicuspid valve; bicuspid valve; quadricuspid valve; hemodynamics

INTRODUCTION

Aortic valve anatomy can vary over a wide range of morphologies ranging from unicuspid to quadricuspid valve type¹. The most common valve abnormality is the congenital bicuspid valve (BAV) with two functional leaflets¹. BAV occurs in the general population at a rate of 1-2% and is associated with significant complications such as aortic aneurysm and dissection^{2,3}. BAV has several subtypes grouped by the valve leaflet fusion patterns (type I right-left leaflet fusion, RL; type 1 right-non-coronary leaflet fusion, RN; and type 0, or a 'true' bicuspid valve)¹. Additional rarer variants include unicuspid (or unicommisural/monocuspid) and quadricuspid (four leaflets) valves which have been found with an incidence of 0.02% and 0.043%, respectively. Both phenotypes have been associated with aortic stenosis and dilation^{4,5}.

Recently, the effect of valve morphology on 3D blood flow changes in the ascending aorta has been identified as a potential contributing factor to the development of aortic pathologies⁶⁻¹⁰. These studies, based on 4D flow MRI, have shown that the 3D alterations in blood flow in the presence of BAV can result in altered aortic hemodynamics and thus wall shear forces which are suspected to promote aortic remodeling. Prior studies have also directly linked BAV RL and RN fusion patterns to altered aortic hemodynamics^{6,9-11}. Additionally, relationships between valve morphology and aortic pathology have also been shown in previous studies using CTA and MR^{8,12,13}. The purpose of this study was to evaluate changes in aortic hemodynamics in a case series representing the wide range of congenitally abnormal aortic valves including rare unicuspid and quadricuspid cup fusion phenotypes. We hypothesize that the different valve morphologies will directly influence these metrics of ascending aorta hemodynamics.

METHODS

Study Population

Our study cohort was comprised of 14 patients and 14 healthy volunteers. All subjects underwent MRI of the thoracic aorta between November 2011 and August 2012 to evaluate ascending aorta dimensions, aortic valve morphology, and aortic 3D blood flow. Patients with congenitally abnormal valves were retrospectively selected to include three main groups: **group 1**) those with a unicuspid aortic valve (n=3, age: 43 ±4 years, 1 female), **group 2**) those with BAV (n= 9, age: 44±9 years, 4 females), and **group 3**) those with a quadricuspid aortic valve (n=2, 41±1 years old, 1 female). BAV patients were further selected according to the type of leaflet fusion pattern, comprising of those with a right-left coronary leaflet fusion (RL, n=3), a right-noncoronary leaflet fusion (RN, n=3), and a 'true' bicuspid (n=3, defined as two equally-sized leaflets with no raphe, and the orifice opening parallel to the inter-atrial septum, or referenced by Sievers et al. as type 0-lat)¹. In addition, 14 healthy controls with a normal trileaflet aortic valve were included in the study cohort (age: 33.1±7.7 years, 4 females). The study was approved by the Institutional Review Board of Northwestern University (IRB). Informed consent was obtained from all healthy controls. Patients were included in accordance with an IRB protocol which permitted retrospective chart review.

MR Imaging

Cardiac MRI was performed at 1.5T or 3T (Magnetom Espree, Avanto or Skyra, Siemens Medical Systems, Germany). To assess valve morphology and global cardiac function, breath-held, ECG-gated time-resolved (CINE) 2D balanced SSFP images were acquired in all patients¹⁴. For valve imaging, a 2D imaging plane was positioned orthogonal to the aorta at the level of the aortic valve (Figure 1). The 2D CINE SSFP sequence parameters were as follows: spatial resolution = 1.33×1.33 – 1.82×1.82 mm, slice thickness = 6–8 mm, temporal resolution = 11.32–46.72 ms, and a flip angle of 74–78°. For the assessment of aortic blood flow, time-resolved 3D phase-contrast MRI with three-directional velocity encoding (4D flow MRI) was employed to measure 3D blood flow velocities with full volumetric coverage of the thoracic aorta¹⁵. 4D flow MRI was acquired during free breathing using respiratory and prospective ECG gating in a sagittal oblique 3D volume of the thoracic aorta using a velocity sensitivity of 150–200 cm/s along all three directions, a flip angle of 15°, spatial resolution of 1.67 – 3.22×1.77 – 2.38×2.2 – 2.8 mm, and a temporal resolution of 38.4–43.2 ms.

Data Analysis

4D flow data were pre-processed for noise filtering, eddy current correction and velocity aliasing, as previously described¹⁶. 3D visualization of the velocity data was performed using commercial software (EnSight, CEI, Inc. Apex, NC). Flow characteristics were visualized by 3D streamlines (lines tangent to the velocity field) at peak flow systole. 3D streamlines were color coded to reflect the local systolic blood flow velocity. In addition, time-resolved 3D pathlines were calculated to visualize 3D aortic blood flow over the cardiac cycle. To improve anatomic orientation, 2D CINE SSFP images of the aortic valve were co-registered to the 4D flow data as shown in Figure 2 and the supplemental video files.

Flow Jet Patterns

3D streamlines were evaluated to identify the existence of ascending aortic flow jets, defined as the existence of streamlines with high flow velocity > 1 m/s (color coding = red, see Figures 2 and 3) away from the aortic centerline. Flow impingement zones were assessed to evaluate the relationship between the valve morphology and flow pattern. The position of flow impingement was determined by visually identifying the anatomic location (R: right, L: left, A: anterior, P: posterior) of the aortic wall reached by the flow jet at the level of the mid-ascending aorta.

Flow Angle

A 2D analysis plane was positioned in the proximal ascending aorta approximately 2 cm above the aortic valve (Figure 2b, white rectangle). Segmentation of the aortic lumen at each time step was used to quantify the lumen diameter and flow angle. The flow angle, i.e. the angle between the vector orthogonal to the analysis plane (n) and the mean flow vector (q) was calculated using $\theta = \cos^{-1} n \cdot q$ (Figure 2b).

Statistical Analysis—Results are presented as mean \pm standard deviation. Group comparisons were performed using the Kruskal-Wallis test between the control population and the valve disease cohorts. A p value < 0.05 was considered significant.

RESULTS

Patient demographics are summarized in Table 1. Examples of different valve morphologies are shown in Figure 1. The degree of aortic valve stenosis (AS) or insufficiency (AI) did not exceed “mild” for all subjects. The aorta was dilated in all patient groups compared to the trileaflet population with normal aortic size (3.6 ± 0.4 cm vs. 2.6 ± 0.3 cm, $p = 0.005$).

Flow Jet Patterns

Figure 3 illustrates typical systolic aortic 3D flow patterns for all valve types. Normal trileaflet valves (Figure 3, controls on left) showed cohesive streamlines (mostly parallel to the ascending aorta without flow jet impinging on the aortic wall). In contrast, 3D flow visualization for all congenitally abnormal valves showed marked flow derangement. Elevated velocity jets along the aortic wall could be clearly identified and associated with distinct flow impingement locations (Table 1). While all RL-BAV were associated with flow jets directed towards the right anterior aortic wall, RN-fusion and unicuspid valves resulted in flow jet patterns towards the right-posterior or posterior wall. Note that the differences in aortic flow pattern can visually be best appreciated in the supplemental video files.

Flow Angle

Results of flow angle analysis are summarized in Table 1 and Figure 3. Markedly higher flow angles for unicuspid ($47\pm 10^\circ$) and BAV with true and RN fusion patterns ($28^\circ\pm 2$ and $29^\circ\pm 18$, respectively) confirm that aortic flow was directed more towards the aortic wall compared to controls ($7^\circ\pm 1$). Changes in flow angle for RL-BAV and quadricuspid patients were less pronounced ($18^\circ\pm 12$ and $15^\circ\pm 2$, respectively).

DISCUSSION

4D flow MRI was employed to study in-vivo post-valvular flow dynamics in the ascending aorta of patients with congenitally malformed aortic valves. The findings support the hypothesis that variations in valve morphology will exhibit distinct changes in aortic hemodynamics according to the valve structure. In our small cohort of patients we found evidence for distinct changes in flow jet patterns and flow angle between subjects with unicuspid, bicuspid, trileaflet, and quadricuspid valves. Specifically, our findings indicate that the position of flow impingement zones may be directly related to the valve leaflet morphology.

In accordance to recent studies^{6,17}, we found different 3D flow patterns in the ascending aorta of our RL-BAV and RN-BAV patients compared to controls. In addition, even unicuspid and quadricuspid valves with more symmetric valve geometry exhibited clearly visible flow jets and impingement zones as well as marked differences in flow angle compared to tricuspid controls. These findings indicate that differences in aortic hemodynamics can potentially provide correlative (although not causative) evidence for an underlying mechanism behind the heterogenic expression of aortopathy in BAV patients with conjoined RL and RN leaflets^{1,8,13,18}. If altered aortic hemodynamics do indeed contribute to the progression of aortopathy, then the data presented here illustrates a

differentiating characteristic beyond genetic predisposition that might be used for risk stratification and clinical decision making. In contrast to previous studies measuring wall shear forces^{6,19}, we chose to analyze our cohort using simple hemodynamic metrics that may act as proxy metrics of wall forces, such as the average blood flow angle in the ascending aorta and flow/wall impingement location. This is similar to efforts to simplify burden of WSS measurement, as highlighted in the recently published studies investigating the concept of ‘flow displacement’^{19,20}

An inter-leaflet raphe or false commissure was present in the unicuspid, RL, and RN patient cohorts. It is notable that flow impingement was observed at the aortic wall opposite to the fused leaflets in those patients with a raphe. Differences in leaflet fusion patterns may thus play a role in changing the flow impingement zone and aortic regions experiencing increased wall shear forces.

It is important to note that even without aortic valve stenosis, the morphology of BAV leads to changes in flow patterns beyond those with healthy trileaflet valves⁶. For example, Della Corte et al. reported a decreased opening angle and restricted motility of valves as the main source of abnormal flow pattern which was also correlated to greater aorta growth rates in BAV patients⁹. In addition, the correlation between the type of leaflet fusion and the local expression of aortopathy has been demonstrated⁸. While RN fusion has been associated with aortic arch aneurysms, the RL fusion has been correlated with aortic root dilatation¹³. In this context, previous studies by Barker et al. and Hope et al. demonstrated a correlation between leaflet fusion pattern and flow direction (RL and RN fusion resulting in right anterior and left posterior flow jet patterns, respectively)^{6,7}. In the present study, the same flow impingement pattern was observed in patients with RL and RN valve fusion. If flow eccentricity is a contributor to aneurysm formation in BAV patients, increased flow angle and the anatomical location of flow impingement might help to predict the specific aorta wall segments at higher risk for dilatation.

The findings of this study indicate that 4D flow MRI and the possibility for a comprehensive assessment of aortic hemodynamics has the potential to improve the evaluation of an abnormal aortic valve and its impact on aortic flow and geometry. Nevertheless, we believe that knowledge of the valve morphology (fusion pattern, presence of stenosis or insufficiency) provides an important addition to information on regional aortic hemodynamics. Specifically, the structure-function relationship between valve abnormality, changes in aortic hemodynamics and development of aortopathy and not yet fully understood. Further longitudinal studies are needed to determine which combination of parameters (i.e. risk score) provides the best predictive value for patient prognosis.

An obvious limitation of this study is related to the small sample sizes of the individual valve morphology groups which precluded the use of subgroup statistical tests to quantify differences between specific morphologies of congenitally abnormal valves and trileaflet controls. In addition, the control group had smaller aortic diameters than the patients. Nevertheless, the data indicates a notable relationship between valve phenotype and eccentric flow impingement zone. To our knowledge this is the first study providing a detailed

comparison of aortic flow characteristics in a wide range of congenitally abnormal valves including rare subtypes such as those with unicuspid and quadricuspid morphologies.

3D analysis methods are needed for measuring and comparing the alignment of the aortic outflow jet relative to the curved axis (centerline at each level) of the ascending aorta, distinguishing jet flow angles from jet flow offset relative to local center line. In addition, new methods are needed for determining whether or not certain ascending aortic geometries are related to valve morphology and whether the flow jet angle and its direction relative to the aortic geometry is a determinant of altered hemodynamics. Application of these methods in larger patient cohorts are warranted to distinguish cause and effect among flow impingement zones, flow angle, aortic dilatation and BAV cusp fusion phenotype.

In conclusion, this study provides evidence to support the hypothesis that alterations in 3D aortic hemodynamics are closely linked with the morphology of congenitally abnormal aortic valves. Specifically, the measurement of outflow angle and the observation of the flow impingement regions were different between the valve phenotypes included in this study. Future studies in larger cohorts and longitudinal follow-up are warranted to further evaluate the implications for the development and progression of aortic disease.

Supplementary Material

Refer to Web version on PubMed Central for supplementary material.

ACKNOWLEDGMENTS

The authors also gratefully acknowledge preliminary review of the manuscript by Amir Davarpanah.

Grant support: NIH NHLBI grant R01HL115828, DFG (German Research Foundation) SCHN-1170/2-1 and SIR Foundation Pilot Research Grant. American Heart Association Scientist Development Grant 13SDG14360004. Additional support by the Northwestern's Bicuspid Aortic Valve Program at the Bluhm Cardiovascular Institute.

REFERENCES

1. Sievers H-H, Schmidtke C. A classification system for the bicuspid aortic valve from 304 surgical specimens. *J Thorac Cardiovasc Sur.* 2007; 133(5):1226–1233.
2. Fedak PWM, Verma S, David TE, Leask RL, Weisel RD, Butany J. Clinical and pathophysiological implications of a bicuspid aortic valve. *Circulation.* 2002; 106(8):900–904. [PubMed: 12186790]
3. Ward C. Clinical significance of the bicuspid aortic valve. *Heart.* 2000; 83(1):81–85. [PubMed: 10618341]
4. Feldman BJ, Khandheria BK, Warnes CA, Seward JB, Taylor CL, Tajik AJ. Incidence, description and functional assessment of isolated quadricuspid aortic valves. *Am J Cardiol.* 1990; 65(13):937–938. [PubMed: 2181849]
5. Novaro GM, Mishra M, Griffin BP. Incidence and echocardiographic features of congenital unicuspid aortic valve in an adult population. *J Heart Valve Dis.* 2003; 12(6):674–678. [PubMed: 14658804]
6. Barker AJ, Markl M, Burk J, Lorenz R, Bock J, Bauer S, Schulz-Menger J, von Knobelsdorff-Brenkenhoff F. Bicuspid aortic valve is associated with altered wall shear stress in the ascending aorta. *Circulation Cardiovascular imaging.* 2012; 5(4):457–466. [PubMed: 22730420]
7. Hope MD, Hope TA, Meadows AK, Ordovas KG, Urbania TH, Alley MT, Higgins CB. Bicuspid aortic valve: four-dimensional MR evaluation of ascending aortic systolic flow patterns. *Radiology.* 2010; 255(1):53–61. [PubMed: 20308444]

8. Kang J-W, Song HG, Yang DH, Baek S, Kim D-H, Song J-M, Kang D-H, Lim T-H, Song J-K. Association Between Bicuspid Aortic Valve Phenotype and Patterns of Valvular Dysfunction and Bicuspid Aortopathy Comprehensive Evaluation Using MDCT and Echocardiography. *JACC: Cardiovascular Imaging*. 2013; 6(2):150–161. [PubMed: 23489528]
9. Della Corte A, Bancone C, Conti CA, Votta E, Redaelli A, Del Viscovo L, Cotrufo M. Restricted cusp motion in right-left type of bicuspid aortic valves: A new risk marker for aortopathy. *The Journal of thoracic and cardiovascular surgery*. 2011
10. Bissell MM, Hess AT, Biasioli L, Glaze SJ, Loudon M, Pitcher A, Davis A, Prendergast B, Markl M, Barker AJ, Neubauer S, Myerson SG. Aortic dilation in bicuspid aortic valve disease: flow pattern is a major contributor and differs with valve fusion type. *Circulation Cardiovascular imaging*. 2013; 6(4):499–507. [PubMed: 23771987]
11. Vergara C, Viscardi F, Antiga L, Luciani GB. Influence of bicuspid valve geometry on ascending aortic fluid dynamics: a parametric study. *Artificial organs*. 2012; 36(4):368–378. [PubMed: 21995712]
12. Fazel SS, Mallidi HR, Lee RS, Sheehan MP, Liang D, Fleischman D, Herfkens R, Mitchell RS, Miller DC. The aortopathy of bicuspid aortic valve disease has distinctive patterns and usually involves the transverse aortic arch. *The Journal of thoracic and cardiovascular surgery*. 2008; 135(4):901–907. e902. [PubMed: 18374778]
13. Schaefer BM, Lewin MB, Stout KK, Gill E, Prueitt A, Byers PH, Otto CM. The bicuspid aortic valve: an integrated phenotypic classification of leaflet morphology and aortic root shape. *Heart*. 2008; 94(12):1634–1638. [PubMed: 18308868]
14. Malaisrie SC, Carr J, Mikati I, Rigolin V, Yip BK, Lapin B, McCarthy PM. Cardiac magnetic resonance imaging is more diagnostic than 2-dimensional echocardiography in determining the presence of bicuspid aortic valve. *The Journal of thoracic and cardiovascular surgery*. 2011
15. Markl M, Harloff A, Bley TA, Zaitsev M, Jung B, Weigang E, Langer M, Hennig J, Frydrychowicz A. Time-resolved 3D MR velocity mapping at 3T: improved navigator-gated assessment of vascular anatomy and blood flow. *J Magn Reson Imaging*. 2007; 25(4):824–831. [PubMed: 17345635]
16. Bock, J.; Kreher, BW.; Hennig, J.; Markl, M. Optimized pre-processing of time-resolved 2D and 3D phase contrast MRI data. Berlin, Germany: May. 2007 p. 3138
17. Hope MD, Hope TA, Crook SES, Ordovas KG, Urbani TH, Alley MT, Higgins CB. 4D flow CMR in assessment of valve-related ascending aortic disease. *JACC-Cardiovascular Imaging*. 2011; 4(7):781–787. [PubMed: 21757170]
18. Fernandes SM, Khairy P, Sanders SP, Colan SD. Bicuspid aortic valve morphology and interventions in the young. *J Am Coll Cardiol*. 2007; 49(22):2211–2214. [PubMed: 17543642]
19. Hope MD, Wrenn J, Sigovan M, Foster E, Tseng EE, Saloner D. Imaging biomarkers of aortic disease: increased growth rates with eccentric systolic flow. *J Am Coll Cardiol*. 2012; 60(4):356–357. [PubMed: 22813616]
20. Sigovan M, Hope MD, Dyverfeldt P, Saloner D. Comparison of four-dimensional flow parameters for quantification of flow eccentricity in the ascending aorta. *J Magn Reson Imaging*. 2011; 34(5): 1226–1230. [PubMed: 21928387]

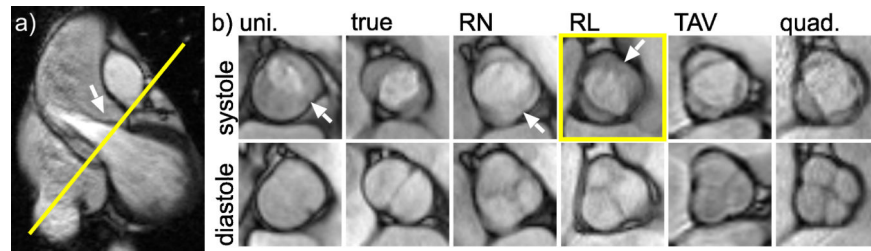


Figure 1.

(a) Position of the 2D SSFP imaging plane for the assessment of the aortic valve. (b) Spectrum of leaflet anatomies examined: A unicuspid (uni.), true bicuspid (true), a right-noncoronary (RN) leaflet fusion, a right-left coronary (RL) leaflet fusion, a normal trileaflet aortic valve (TAV), and a quadricuspid (quad.) valve are shown at systole and diastole. Arrows show the location of the raphe (if present) between the conjoined leaflets. The incomplete opening of the conjoined RL leaflet (yellow box, arrow) is also observed in the left ventricular outflow tract view (a, arrow).

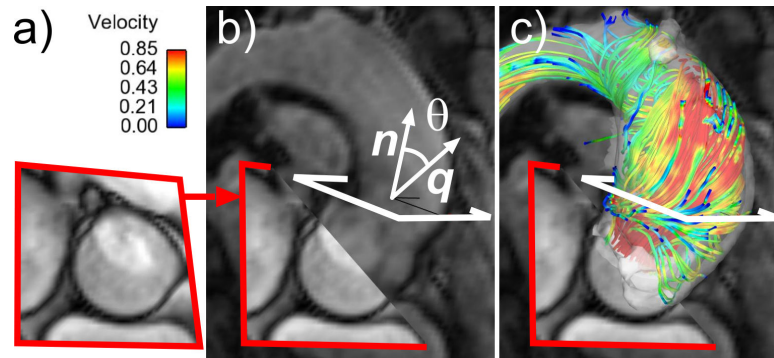


Figure 2.

Data analysis strategy. A 2D SSFP CINE image of a unicuspid aortic valve (a) was co-registered with the 4D flow data and 3D flow visualization (c). An analysis plane distal to the aortic valve (b) was used to compute the systolic flow angle, θ , as the angle between the net systolic flow, q , and the analysis plane unit normal, n . The streamline visualization (c) shows an abnormal flow jet in an example unicuspid patient.

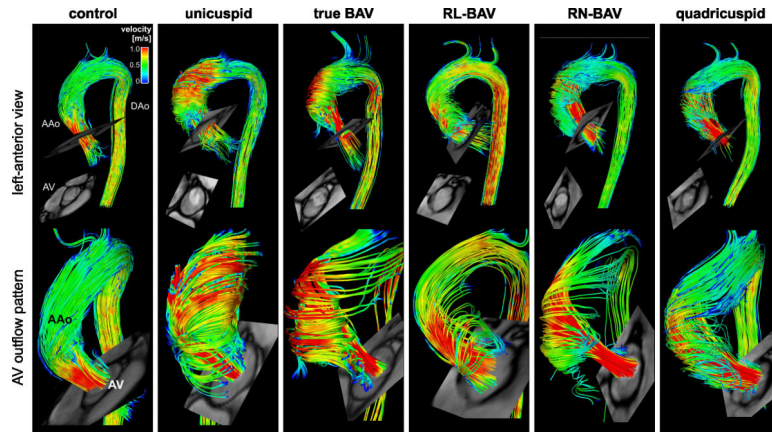


Figure 3. Relationship between valve morphology and 3D flow patterns distal to the aortic valve (AV). Note the different systolic AV outflow flow jet patterns and wall impingement zones between different valve groups. Differences in aortic hemodynamic can be best appreciated in the supplemental video files 1-6.

Table 1

Demographics and Flow Quantification

	congenitally deformed valves (n=14)						<i>p-value</i> controls vs. all patients
	control		bicuspid				
	tricuspid	unicus pid	true (lat)	right-non	right-left	quadricuspid	
n (female)	14(4)	3(1)	3(2)	3(2)	3(0)	2(1)	-
Age	33.1±7.7	43.1±4.0	39.1±2.9	42.2±10.8	51.9±9.1	40.6±0.5	0.030
AAo Diameter (cm)	2.6±0.3	3.9±0.6	3.4±0.1	3.4±0.7	3.9±0.5	3.5±1.1	0.005
Flow Angle(°)	7±1	47±10	28±2	29±18	18±12	15±2	0.001
Flow Imp. (A,R,P,L)	-	P	RA,RP,-	P	RA	RA,-	-

(R: right, L: left, A: anterior, P: posterior, RA: right anterior, LA: left anterior, RP: right posterior, LP: left posterior). The p-value represents differences between normal tricuspid controls (n=14) and the entire group of patients with congenitally altered valves (n=14).